LJMU Research Online

Eslami Mjad, A and Ekere, NN

 Numerical analysis on thermal crack initiation due to non-homogeneous solder coating on the round strip interconnection of photo-voltaic modules

http://researchonline.ljmu.ac.uk/id/eprint/15726/

Article

"Numerical Analysis on Thermal Crack Initiation due to Non-Homogeneous Solder Coating on the Round Strip Interconnection of Photo-voltaic Modules"

Alireza Eslami Mjad[a,*] and Nduka Nnamdi Ekere[a]

[a]School of Engineering, Faculty of Science and Engineering, University of Wolverhampton Shifnal Road, Priorslee, Telford Shropshire TF2 9NN, UK

Abstract

Solar energy is one of the most widely used renewable energy sources, with photo-voltaic (PV) solar cells/panels now utilized as an important energy source. The strip interconnection between solar cells (used for collecting current from solar cells) is a key PV module component; as poor interconnection reliability can lead to PV module failure. Multi-Busbar is a new type of interconnection which incorporates several round copper wires to help increase the energy conversion and transmission efficiency of PV modules and also to reduce the material costs. The non-homogeneity of the solder coating on the wires (resulting from manufacturing process faults), is one of the main factors that is responsible for the poor connections between the wire and the silver pads; which adversely impacts on the interconnection strength and long term reliability. This paper concerns an investigation of the effect of solder coating non-homogeneity on the thermo-mechanical response of round wires used for PV module interconnections. The study evaluates the two main parameters of non-homogeneity (out of centre value and direction), and also investigates the effect of geometrical parameters. The Extended Finite Element Method in ABAQUS software was used to determine the micro-crack initiation temperature and location for a given joint design. The results show that the cracking temperature is most affected by the direction of solder coating non-homogeneity and the downward vertical direction of out of centre positioning of copper in the solder coating leads to the most reduction in cracking temperature (up to 21%).

Keyword: PV Module, Multi-Busbar interconnection, Non-Homogeneity of Solder Coating, Crack Initiation, Reliability.

1. Introduction

Ribbon interconnections are one of the main components of PV Modules which connect the individual crystalline silicon solar cells and transmit and conduct their electrical current to external circuits. The design of the ribbon interconnection therefore has a direct influence on the efficiency of

* Corresponding author. Tel.: +44 (0)1902 321 703; fax: +44 (0)1902 321 459.
E-mail addresses: a.e.majd@wlv.ac.uk (Alireza Eslami Majd), ndyekere@wlv.ac.u (Ndy Ekere)

the PV module (in terms of energy conversion and transmission) and the long term reliability. The configuration of the interconnection influences the Shading on the PV Cells and the partial shading loss (with partial shading, one part of the solar panel generates lower amount of energy as compared to the other non-shaded part) reduces the performance and efficiency of PV Modules (Pareek et al., 2017). Many efforts focussed on developing new joining materials have been reported, such as that on electrically conductive adhesive (ECA) joints or conductive paste (CP)-assisted low-temperature soldering (CALS) as an adhesive layer to connect the strips to the cells (Song, et al., 2019) and although this leads to a cheaper interconnection solution (use of less solder materials), the interconnections do not have the required high shear strength.

The Multi-Busbar (MBB) Connector is one of the innovative concepts for strip interconnection and solar cell tabbing. The aim of the MBB design is to increase the number of busbars and to reduce the busbars' width and finger cross sections (Schneider et al., 2006). In comparison with conventional interconnection method, the use of the MBB technology leads to a reduction in the series resistance losses, due to the increased number of current paths and the associated uniform current distribution (Schindler et al., 2013) and (Walter et al., 2014). For example, by using 15 wires instead of three traditional rectangular busbars, the finger length can be reduced from 25mm to 5mm and the width of the finger can also be reduced from 50 µm to 17 µm (Braun et al., 2013). This reduction in Ag-paste area results in bringing down the cost of PV modules, by reducing the consumption of silver by up to 89%. In addition, the use of rounded edge wires in the MBB design helps to reduce the shadowing loss as most of the incident light can be reflected onto the wafer surface; helping to increase the power output as well as the efficiency of PV (Braun et al., 2012). However, the MBB Connector has one unresolved design/manufacture challenge; the problem associated with the non-homogeneity of solder coating that is produced around the Cu-wire which can result in weaker solder joints and interconnections (Walter et al., 2014). Figure 1, shows the cross-sectional views of round copper wires with homogeneous and non-homogeneous solder coating.
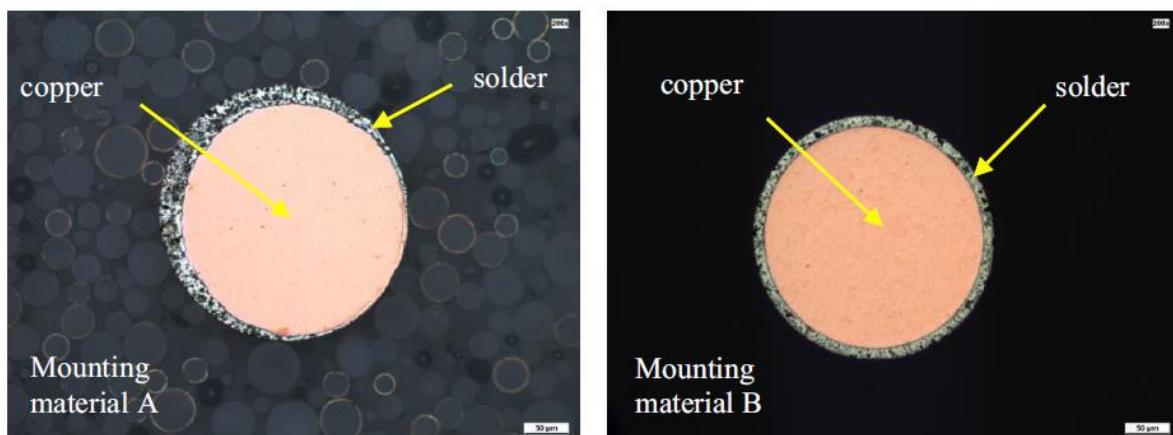
Figure 1 Round wire with non-homogeneous (left) and homogeneous (right) solder coating (Walter et al., 2014)

Thermal stress due to coefficient of thermal expansion (CTE) mismatch between interconnection materials and PV module materials can lead to early interconnection failure and adversely impact on the reliability of the PV module interconnection (O. Ogbomo et al., 2018) and (Zarmai et al., 2016). Indeed, in high temperatures, the weaker MBB solder joint connection area subjected to the thermal stress can develop micro cracks. Previous studies show that the cracks are developed mainly in the contact surface of the strip interconnection and the contact condition can adversely affect the performance of the whole module in terms of power output (Jeong, et al., 2012) and (Itoh et al., 2014). Indeed, the crack developed induces contact resistivity between the Cu ribbon interconnection and cell; resulting in cell-to-module (CTM) loss, hot spot and eventually the disconnection of the bus bar line which consequently results in DC arc (Itoh et al., 2014) and (Tae-hee Jung, 2014).

Rendler et al. have investigated the deformation of cell and thermomechanical stress in both cell and interconnecting wire of MBB PV modules. They found by using lower diameter of wires and by reducing the Young's modulus or the yield strength of the copper, the thermomechanical stress in a solar cell is decreased. They also recognized that the maximum stress in the wires occurs at the edge of the outermost contact pads on both sides of the solar cell (Rendler et al., 2016, 2018). This important region of the solder joint material is where the Intermetallic compound (IMC) is formed. Intermetallic compounds (alloys) form whenever two different metals are soldered together and grow as solid phases during the solidifying of solders on the interface between the solder alloy and its bonding pads (Pecht, 1993). Generally, the thermal fracture of a solder connection due to crack propagation is divided into two distinct modes. Firstly, inside a solder joint (solder-controlled fracture) due to the growing grain size of solder and decreasing bonding strength during thermal cycles, a crack progresses at the interface of large grain. Secondly, at the interface of the solder with interconnection material layers by generating Intermetallic Compounds (IMC) layer such as Cu_5Sn_6 and Ag_3Sn due to the dissolution of Ag/Cu in the solder and the formation of a brittle layer (Itoh et al., 2014). Experimental observations show that the fractures and straight crack path are located on the component side of the solder interconnections (beneath die edge) (Li et al., 2012). Consequently, it is obvious that the IMCs layers in the solder region boundaries play a significant role in the nature of failure and subsequently life time and reliability of solder interconnection. The focus of this study is on the effect of non-homogenous coatings on the strength of brittle micro-cracking in the Intermetallic Compound (IMC) of solder joint in PV module's interconnection.

2. Methodology and Simulation

In this study, we investigate the effect of out of centre of solder coat around copper wire on the crack initiation temperature. Extended Finite Element Method (XFEM) in ABAQUS 6.17 has been utilized to analyse the hot temperature crack initiation (ABAQUS Theory Manual, 2017). XFEM is based on the partition of unity method, and this numerical technique extends conventional finite

96 element method and allows local enrichment discontinuous functions to be combined with the

97 conventional finite element approximation (Sivakumar & Maji, 2016). One of the main advantages of

98 this method is avoiding any need for re-meshing or geometric crack modelling in numerical

99 simulation, while generating discontinuous fields along a crack and around its tip (Mohammadi,

100 2008). Unlike conventional FE methods, with the XFEM method there is no need for specifying the

101 location of the crack beforehand. This means that XFEM models a crack within an element as an

102 enriched feature by adding degrees of freedom in elements with special displacement functions

103 (ABAQUS Theory Manual, 2017).

104   In this study, 2D symmetrical simulation of interconnection strips with four-node plane strain

105 elements (CPE4) is performed as this requires less Computational processing and storage compared to

106 3D simulation modelling. Altogether, 82 interconnection strip models were simulated in ABAQUS

107 CAE.

108   Based on Multi-Busbar Connector Prototype specifications published by (Walter et al., 2014), the

109 diameter of copper ribbon and width of silver pad are assumed to be 270 µm and 450 µm,

110 respectively; and the thickness of silver pad and silicon cell are 20 µm and 220 µm (Note: in order to

111 achieve stable response, the gaps between the interconnection strips were considered to be 6mm). To

112 investigate effect of geometrical parameters, four different solder coating thickness (15 µm, 20 µm,

113 25 µm and 30 µm) were evaluated. In addition, the effect of IMC layer thickness (silver pad interface)

114 was investigated; with four different IMC layer thickness considered (1 µm, 2 µm, 3 µm and 4 µm

115 was used to reflect wide range of soldering temperature). However, the IMC layer thickness on the

116 copper wire core interface is assumed to be 2 µm and symmetry boundary conditions are applied for

117 the bottom of silicon cell. The top edge of Ethylene Vinyl Acetate (EVA) which in contact with the

118 glass protective sheet in PV Module is considered closed in X and Y direction (i.e. no X and Y

119 direction movement is assumed). The temperature of whole solar cell has been increased linearly and

120 isothermally to the crack initiation temperature. Figure 2, shows the discretization and meshing

121 method used in the study and the configuration for the Copper core, Solder Joint, Intermetallic

122 Compound (IMC), Silver Pad, EVA and Silicon cell. A very fine mesh size   of 1 µm was used for

123 investigating the effect of the IMC layer thickness on the silver pad interface; and to determine the

124 crack initiation temperature and location of micro-crack.

125   To meet the requirements of the theory of Linear Elastic Fracture Mechanics (LEFM) which is

126 basis of XFEM for investigation of crack propagation, the IMC layer between solder and silver pad is

127 assumed as a brittle elastic material; whilst all other metallic materials in the PV Module (silver,

128 copper and solder) are considered to have plastic behaviour. Based on the models for traction-

separation laws, different of types of strain and stress components (MAXPS / MAXPE[2], MAXS / MAXE [3] and QUADS/ QUADE[4]) can be used to control damage initiation. In this study, the maximum nominal stress (MAXS) of Shear and Tensile components is considered as the controlling parameters for the damage initiation. This means that the damage (crack) is initiated when these components exceed the defined limits. Then, the initiated crack will be evaluated as Fracture Energy formulations which can be formed by the parameter of Fracture Toughness and Elastic Modulus (Du, 2009).

Table 1 shows the mechanical properties of materials used in the simulation. The temperature dependency of the thermal coefficient of expansion was considered for the Silver, Solder, IMC and copper materials; and the temperature dependency of the Young's Modulus and plastic behaviour was also considered for Solder as shown in Table 2.
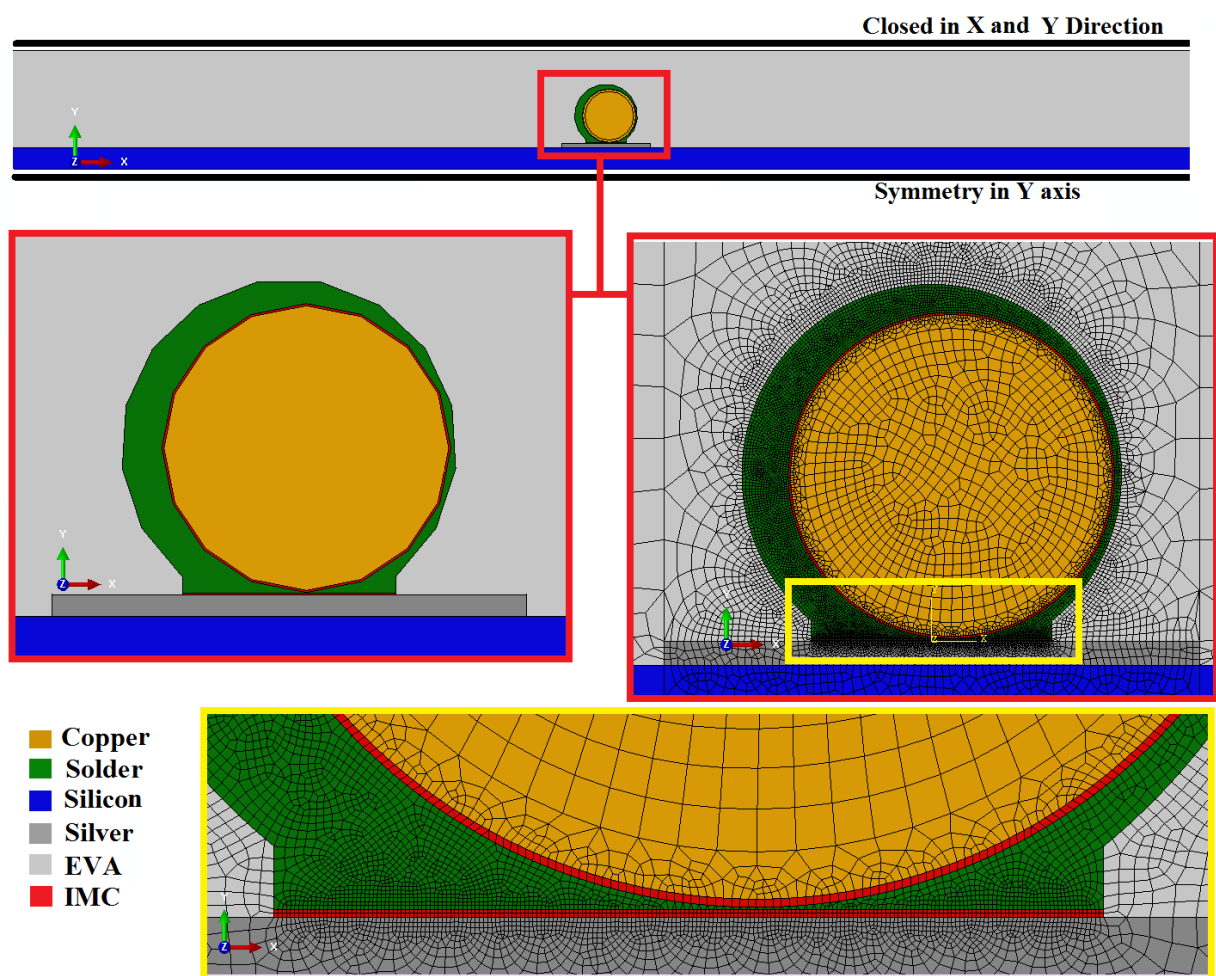
Figure 2 Applied mesh and material arrangement of the PV module Cell in the top interconnecting area

---

[2] Maximum principal stress (MAXPS) and maximum principal strain (MAXPE)
[3] Maximum nominal stress (MAXS) and maximum nominal strain (MAXE)
[4] Quadratic nominal stress (QUADS) and quadratic nominal strain (QUADE)

Table 1 Mechanical Properties of Material used in the FEM simulation of strip interconnection

Parameter (unit)	Material					
	IMC (SnAg)	Solder Joint	Silver (AZoM, 2001)	Copper (Jing, et al., 2015)	EVA (Department, 2003)	Silicon (Owen-Bellini et al., 2015)
Elastic Modules (MPa)	See Table 2	See Table 2	69	121	11	170
Poisson's Ratio (-)	0.35	0.35	0.365	0.34	0.499	0.28
Yield Stress (MPa)	-	-	43	121	12	170
Shear Strength (MPa) (Deng et al., 2005)	27.6-1.95*H_{IMC}	30	-	-	-	-
Tensile Strength (MPa) (Zhong et al., 2010)	65	78	-	-	-	-
Fracture Toughness (MPa.m^0.5)	7	7	40	30	-	0.83
Thermal Expansion Coefficient (ppm/k)	See Table 2	See Table 2	See Table 2	See Table 2	270	2.6
Plastic Stress-Strain Curve (MPa)	-	See Table 2	43@0.001 120@0.04	121@0.001 186@0.004 217@0.01 234@0.02 248@0.04	-	-

Table 2 Temperature dependent properties of interconnection materials

| Temp. (c)	CTE for Copper (ppm/k) (Taulaukian et al., 1975) (Interpolated)	CTE for Silver (ppm/k) (Taulaukian et al., 1975) (Interpolated)	CTE for Solder (ppm/k) (49-0.07T) (Li, el al., 2012)	Solder Young's Modulus (MPa) (21.3+0.017T) (Li et al., 2012)	Stress (MPa) (at 0.0, 0.065 Plastic Strain) (Siviour et al., 2005) (Interpolated)
0	16.22	18.67	21.3	49	71, 145
30	16.60	18.98	21.81	46.9	52, 131
60	16.91	19.20	22.32	44.8	16, 110
90	17.22	19.42	22.83	42.7	-
120	17.53	19.65	23.34	40.6	-
150	17.76	19.91	23.85	38.5	-

145   The schematic view of cross section of the round ribbon interconnector presented in Figure 3,

146   shows that S_e (the molten solder area) located between the lower end of strip interconnection and the

147   silver pad is displaced sideways to the both left and right corners of interconnect strip; thereby

148   increasing the contact area between the strip interconnection and silver pad. The mathematical

149   expressions used for calculating the extra contact length X_m between the solder joint and the Silver

150   pad is given by equation eq. #5. If we assume that the Solder Area S_e with height H_e is sub-divided

151   into triangular areas S_m; then the derivation of the extra contact length X_m is as detailed in eq. #1 - #5.

152   To investigate the effect of solder joint height on the strength of the strip interconnection, four
153   different molten solder heights H_e was considered (i.e. H_e was varied from 25%, 37.5%, 50% to
154   62.5% of solder coating thickness).
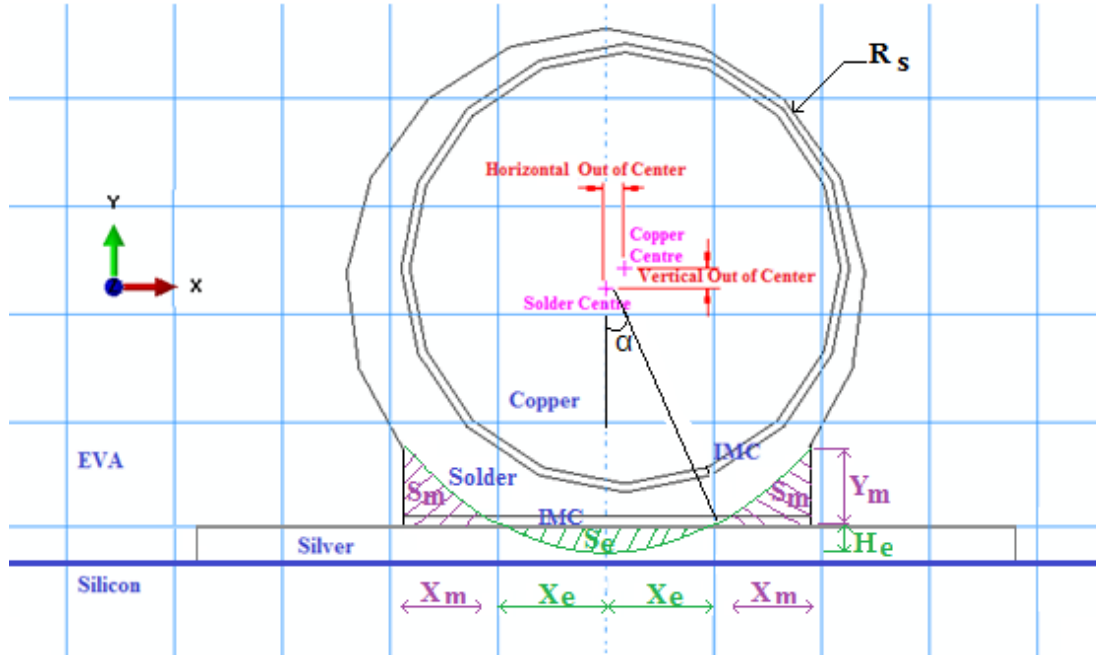
155
156   Figure 3 Cross section of round ribbon interconnector with view of vertical and horizontal out of centre

$Eq.1$: $$X_e = \sqrt{R_s^2 - (R_s - H_e)^2}$$

$Eq.2$: $$tan(\alpha) = \frac{X_e}{R_s - H_e} = \frac{Y_m}{X_m}$$

$Eq.3$: $$S_e = R_s^2.\alpha - 2.X_e.(R_s - H_e)$$

$Eq.4$: $$S_m = \frac{Y_m.X_m}{2} = \frac{S_e}{2}$$

$Eq.5$: $$X_m = \sqrt{\frac{S_e}{tan(\alpha)}} = \sqrt{\frac{R_s^2.Arctan\left(\frac{\sqrt{R_s^2 - (R_s - H_e)^2}}{R_s - H_e}\right) - \sqrt{R_s^2 - (R_s - H_e)^2}.(R_s - H_e)}{\frac{\sqrt{R_s^2 - (R_s - H_e)^2}}{R_s - H_e}}}$$

3. Results and Discussions

158   This section presents the results from the study on the investigation of the effect of solder coating
159   non-homogeneity on the thermomechanical response of round copper wires used for PV module
160   interconnections and the evaluation of the effect of three geometrical parameters, namely the
161   Intermetallic Compound (IMC) layer thickness, solder joint height and thickness on the strength of the
162   interconnections.

163   3.1. Crack location

164   The results of the XFEM analysis presented in Figure 4 shows the one-micrometre crack that is

165   initiated in the IMC layer between the solder joint material and silver pads. For all the geometrical

166   parameters considered in the study, the results show that the highest stress accumulation (and the

167   micro-crack initiation), occurs at the edge of the IMC layer interface between the solder joint and

168   silver pad. . The results also show that the crack propagation is in the parallel direction to the silver

169   pad. The material properties presented in Table 2, show that the micro-crack at the interface between

170   the solder joint and silver pad is caused by the high coefficient of thermal expansion (CTE) mismatch

171   between solder joint and silicon layer.

172   Figure 5 shows the Von Mises stress and shear stress contours in the IMC layer between solder

173   coat and Silver pad at the micro-crack initiation temperature and the crack propagation. Although   the

174   concentration of shear stress in the IMC layer leads to the micro-crack initiation and propagation

175   along the IMC interface layer; further crack progression can be caused by thermal recycling in hot

176   temperature operation which can lead to the disconnection of the strip interconnection from the Silver

177   pad.
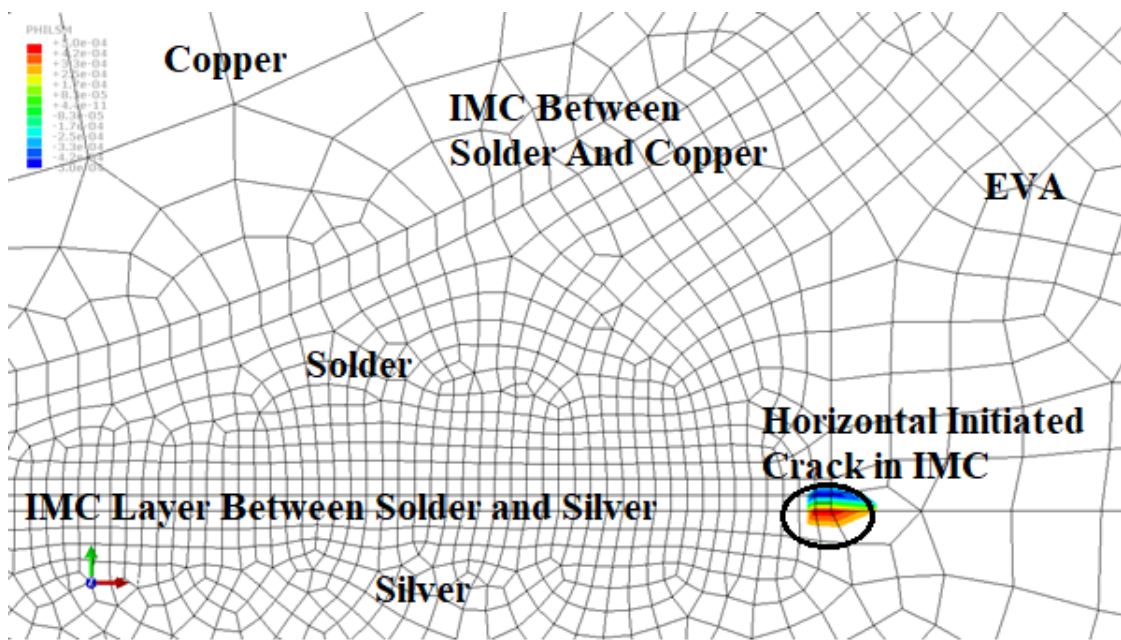
178

179   Figure 4 crack initiation in IMC layer between solder coat and Silver pads
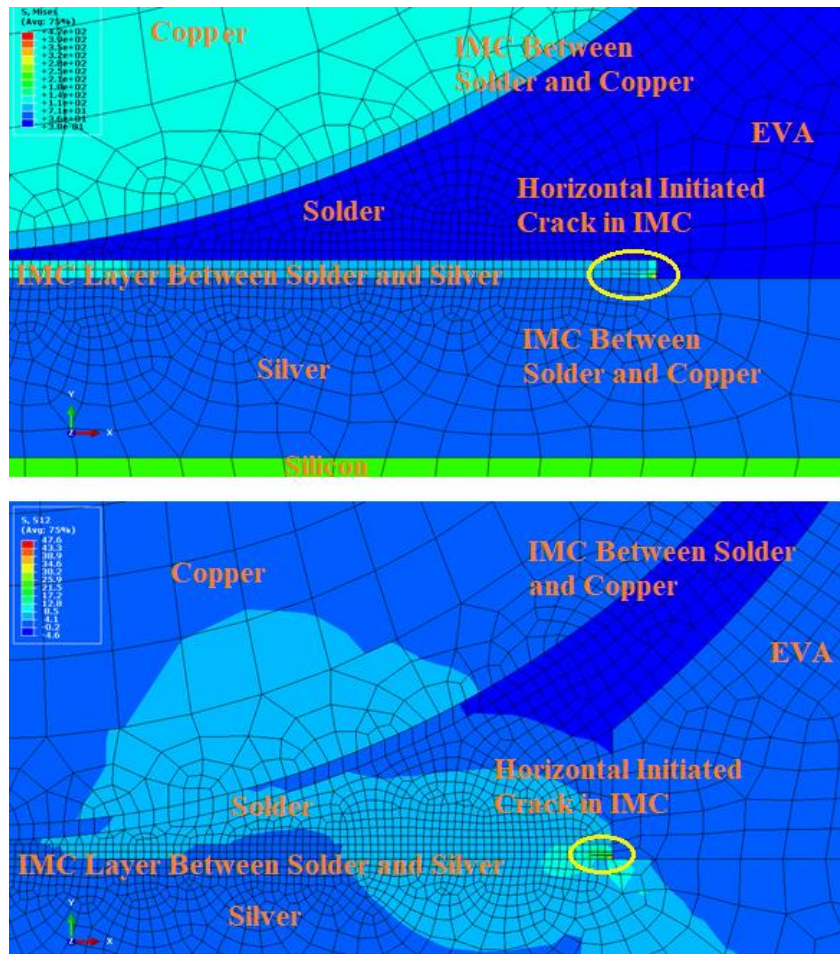
Figure 5 Von Mises Stress (Top) and Shear Stress (Below) Contours in temperatures of micro-cracking of IMC layer between solder coat and Silver pads

3.2. Out of centre positioning of copper in the interconnection strip

Figure 6 shows the crack initiation temperatures for different geometries and out of centre distances in different directions including the upward Y direction (+90 Degrees), the downward Y direction (-90 Degrees), the horizontal (0 Degree) and also the upward and the downward radial directions (-9.5 and +/- 18.5 Degrees). The molten solder height in this graph is considered 50% of solder thickness (10 μm) and the thickness of IMC layer is assumed to be 2 μm. The results of the simulations show that by increasing the out of centre distance (i.e. with more non-homogenous solder coating) in downward directions, the crack initiation strength of the solder joint decreases (Note: the highest rate is for -90 Degree out of centre positioning). This means that for the downward out of centre positioning of the copper inside the coated wire, the crack initiation temperature decreases with increasing non-homogeneity of coating. This is because the narrow solder thickness between copper wire and silicon layer results in an increase in the accumulated strain and thermal stress due to the high thermal coefficient of expansion (CTE) mismatch between the solder and silver materials.. For this reason, the micro-cracks are more likely to occur at the interface between the IMC layer and the silver pad. The results also show that for the upward out of centre positioning of the copper inside the coated wire, the cracking initiation strength of the solder joint is increases with more non-

9

199 homogenous solder coating (increases the micro-crack initiation strength); and the crack initiation
200 temperature is also much higher than those for downward out of centre positioning directions.
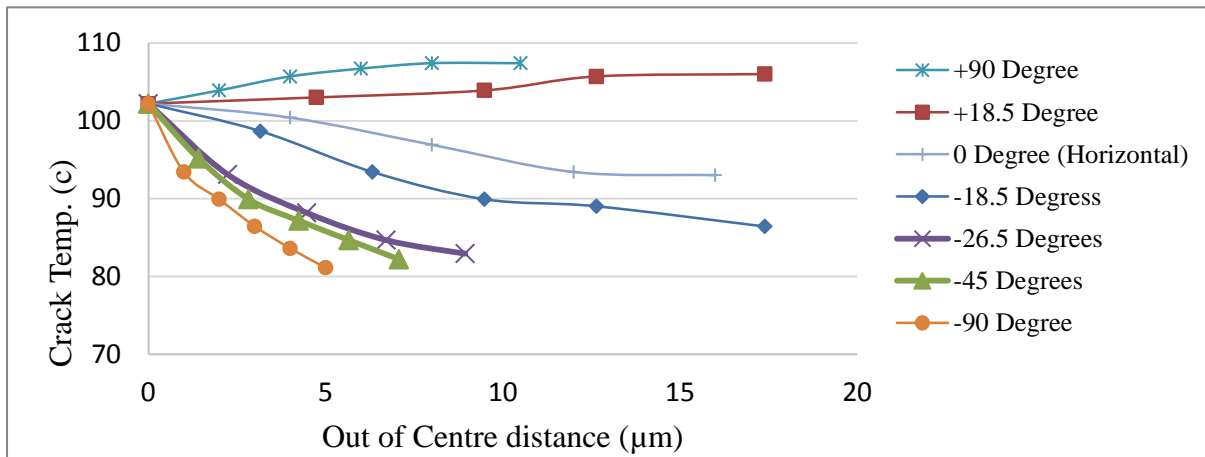
201
202 Figure 6 Temperature of crack initiation for different direction of out of centre distances. The molten solder
203 height is 50% of Solder thickness and the thickness of IMC layer is assumed to be 2 μm.
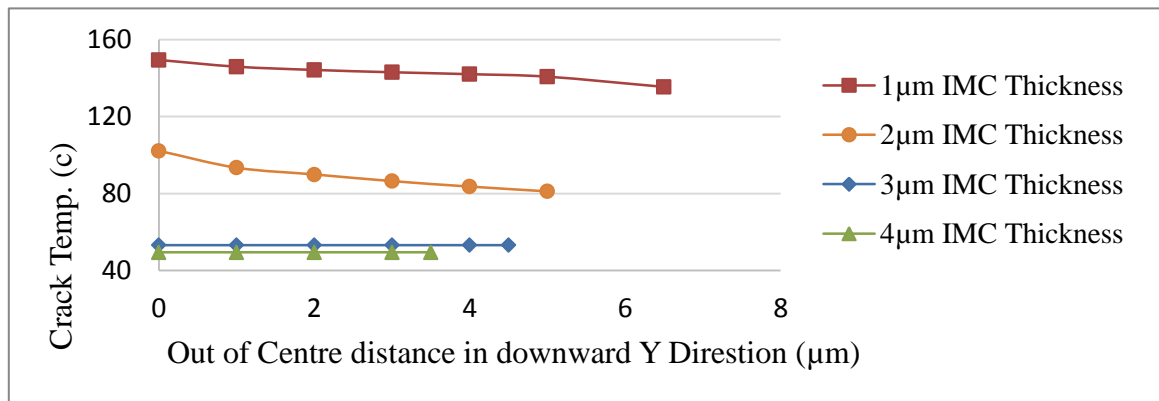
204 3.3. Molten Solder Height

205 Figure 7 shows the effect of the out of centre distance in the downward Y direction (-90 Degrees)
206 for different molten solder heights on the crack initiation temperature. In principle, increasing the
207 molten solder height increases the solder contact between the copper wire and the silver pad and
208 hence lead to more reliable connection; the results in Figure 7 suggests that by increasing the molten
209 solder height and increasing solder contact will actually result in micro-cracks occurring at much
210 lower temperatures. This reduction in the micro-crack initiation temperature can be attributed to the
211 high levels of thermal stress resulting from the coefficient of thermal expansion (CTE) mismatch in
212 the increased solder contact. However, the reduction in the micro-crack initiation temperature due out
213 of centring is mitigated by the increase in solder joint strength; and thereby reducing the impact of out
214 of centring with high molten solder height.
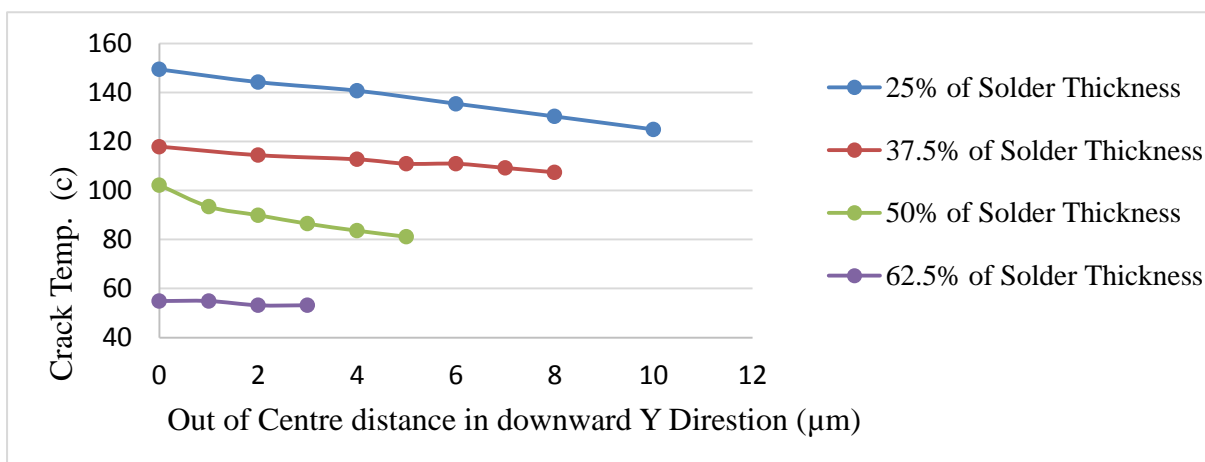
215
216 Figure 7 Temperature of crack initiation via out of centre distances in downward Y direction for different
217 molten solder height. Thickness of IMC layer is considered 2 μm.

218   3.4. Thickness of IMC Interface Layer between strip interconnection and silver pad

219   Figure 8 demonstrates the effect of out of centre distances in downward Y direction (-90 Degrees)

220   on crack initiation temperature for cases where the solder thickness is 20 μm and the molten solder

221   height is 10 μm (i.e. 50% of solder thickness),   with different IMC layer thickness between strip

222   interconnection and silver pad. The results show that solder joints with lower IMC layer thickness

223   exhibited higher strengths than solder joints with higher IMC thickness. The results also show that

224   there is a reduction in the crack initiation temperature with increases in the out of centre positioning;

225   however this is negligible with higher IMC layer thickness.

226
227   Figure 8 Temperature of crack initiation via out of centre distances in downward Y direction for different IMC
228   layer thickness. The molten solder height is 50% of Solder thickness.

229   3.5. Solder Coating Thickness

230   Figure 9 shows the effect of out of centre distances on crack initiation temperature in downward

231   Y direction (-90 Degrees) for cases with 10 μm molten solder height (50% of Solder thickness), IMC

232   layer thickness of 2 μm with different solder thickness. The result shows that for higher solder

233   thickness, increasing the solder thickness reduces the crack initiation temperature; but the effect of out

234   of centre distance on crack initiation temperature is negligible.

235
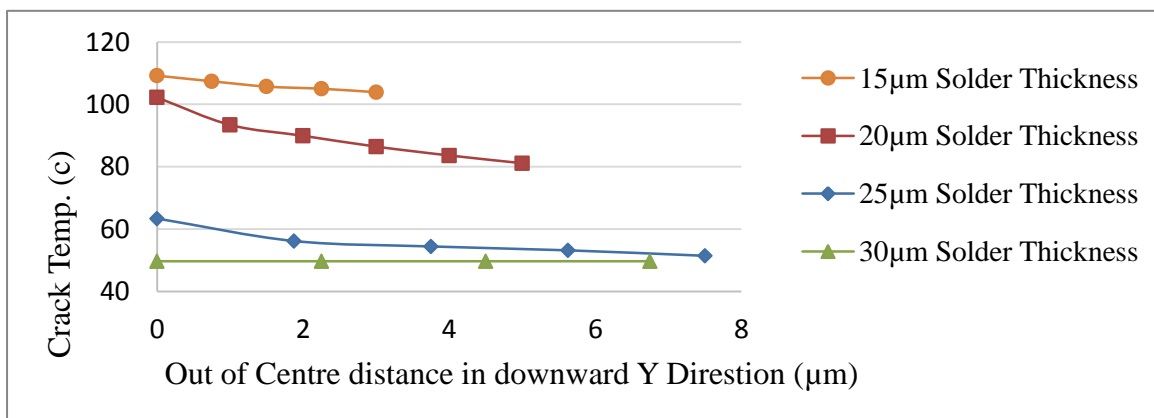
236   Figure 9 Temperature of crack initiation via out of centre distances in downward Y direction for different solder
237   thickness. The molten solder height is 10 μm and the IMC layer thickness is 2 μm.

4. Conclusion

This study presents the results of the Extended Finite Element Method (XFEM) Simulation performed on the round wire used in Multi-Busbar (MBB) strip interconnection of solar PV module to evaluate micro-crack initiation in non-homogenous solder coating at high temperatures. The determination of the conditions for micro-crack initiation in the solder coating on the round wire is important for determining the interconnection design parameters that will ensure long term reliability of the solar PV module. The results from the simulation study would be used for MBB interconnection design and for the evaluation of solar PV module performance and reliability. The study evaluates the two main parameters of non-homogeneity (out of centre value and direction), and also investigates the effect of geometrical parameters including Intermetallic Compound (IMC) layer thickness and solder joint height. The XFEM in ABAQUS 6.17 software package was used to determine the hot temperature required for micro-crack initiation for each joint design. Also, XFEM analysis was used to predict the location of the micro- crack in the IMC layer between solder coating and silver pad.

The results show that the micro-crack is initiated in the parallel direction with silver pad and the initiation temperature is most affected by the direction of solder coating non-homogeneity and the downward vertical direction of out of centre positioning of copper in the solder coating leads to the most reduction in crack initiation temperature (up to 21% reduction was observed for the case 5.5 µm out of centre distance). The results also show that by increasing the amount of molten solder/solder thickness, the micro-crack initiation will take place at a lower temperature due to high thermal stress accumulation in the IMC layer. Also, it was found that at high solder thickness the micro-crack initiation temperature is less affected by non-homogeneity. The results also show that increasing the IMC layer thickness leads to a decrease in the micro-crack initiation temperature threshold and thinner IMC layers are more sensitive with non-homogeneity. The results of the study will also be useful for researchers in evaluating the impact of IMCs layers in the solder region boundaries on solar PV module reliability and in developing design-for-reliability guidelines.

References

ABAQUS, I., 2017. *ABAQUS User's and Theory Manuals; Version 6.17,* s.l.: ABAQUS, Inc.: Providence Rhode Island, RI, USA.

AZoM, 2001. *Silver - Applications and Properties of Silver.* [Online]
Available at: https://www.azom.com/properties.aspx?ArticleID=600

Braun, S. et al., 2013. *The multi-busbar design: an overview.* s.l., s.n., p. 86 – 92.

Braun, S., Micard, G. & Hahn, G., 2012. *Solar cell improvement by using a multi busbar design as front electrode.* s.l., s.n., pp. 227-233.

272 Deng, X., Sidhu, R. j. & Chawla, N., 2005. Influence of reflow and thermal aging on the shear strength
273 and fracture behavior of Sn-3.5Ag Solder/Cu joints. *Metallurgical and Materials Transactions A 36(1),*
274 pp. 55-64.

275 Department, C. U. E., 2003. *Materials Data Book.* Cambridge, UK: Cambridge University Engineering
276 Department Data Books.

277 Du, Z.-z., 2009. *eXtended Finite Element Method (XFEM) in Abaqus.* [Online]
278 Available at: http://www.simulia.com/download/rum11/UK/Advanced-XFEM-Analysis.pdf

279 Itoh, U. et al., 2014. *Solder joint failure modes in the conventional crystalline Si module.* s.l., s.n.

280 Jeong, J.-S., Park, N. & Han, C., 2012. Field failure mechanism study of solder interconnection for
281 crystalline silicon photovoltaic module. *Microelectronics Reliability.*

282 Jing, X. et al., 2015. *Effect of pre-CMP annealing on TSV pumping in thermal budget and reliability
283 test.* Hsinchu, Taiwan, IEEE 22nd International Symposium on the Physical and Failure Analysis of
284 Integrated Circuits.

285 Karppinen, J., Laurila, T., Ka, J. & Li, J., 2012. Reliability of Lead-Free Solder Interconnections in
286 Thermal and Power Cycling Tests. *IEEE TRANSACTIONS ON COMPONENTS AND PACKAGING
287 TECHNOLOGIES, VOL. 32, NO. 2.*

288 Mohammadi, S., 2008. *Extended Finite Element Method: For Fracture Analysis of Structures.*
289 s.l.:Wiley/Blackwell.

290 O. Ogbomo, O., H. Amalu, E., Ekere, N. & P.O., O., 2018. Effect of operating temperature on
291 degradation of solder joints in crystallin esilicon photovoltaic modules for improved reliability in hot
292 climates. *Solar Energy 170,* p. 682–693.

293 Owen-Bellini, M., Zhu, J., R. Betts, T. & Gottschalg, R., 2015. *Thermo-Mechanical Stresses of Silicon
294 Photovoltaic Modules.* Bangor, United Kingdom, s.n.

295 Pareek, S., Chaturvedi, . N. & Dahiya, R., 2017. Optimal interconnections to address partial shading
296 losses in solar photovoltaic arrays. *Solar Energy 155,* p. 537–551.

297 Pecht, M., 1993. *Soldering processes and equipment.* s.l.:Wiley-IEEE. p. 18. ISBN 978-0-471-59167-2. .

298 Rendler, L. C. et al., 2016. *Mechanical stress in solar cells with multi busbar interconnection-
299 Parameter study by FEM simulation.* s.l., s.n.

300 Rendler, L. C., Walter, J., Goldenberg, S. & Bein, A., 2018. Mechanical and electrical properties of
301 wave-shaped wires for low-stress interconnection of solar cells. *Solar Energy Materials and Solar
302 Cells 176,* p. 204–211.

303 Schindler, S. et al., 2013. *Soldering process and material characterization of miniaturized contact
304 structures of a newly developed multi busbar cell metallization concept.* s.l., s.n., p. 480–483.

305   Schneider A, Rubin L & Rubin G, 2006. *Solar Cell Efficiency Improvement by New Metallization*
306   *Techniques - the Day4 Electrode Concept.* Wikoloa, Hawaii, USA, 4th IEEE World Conference on
307   Photovoltaic Energy Conversion.

308   Sivakumar, G. & Maji, V., 2016. Simulation of crack propagation in rocks by XFEM. *Recent Advances*
309   *in Rock Engineering (RARE 2016).*

310   Siviour, C. R., Walley, S., Proud, W. & Field, J., 2005. Mechanical properties of SnPb and lead-free
311   solders at high rates of strain. *Journal of Physics D: Applied Physics,* p. 4131–4139.

312   Song, H.-J.et al., 2019. Conductive paste assisted interconnection for environmentally benign
313   leadfree ribbons in c-Si PV modules. *Solar Energy 184,* pp. 273-280.

314   Tae-hee Jung, H.-e. S. H.-k. A. G.-h. K., 2014. A mathematical model for cell-to-module conversion
315   considering mismatching solar cells and the resistance of the interconnection ribbon. *Solar Energy*
316   *103,* p. 253–262.

317   Taulaukian, Y., Kirby, R., Taylar, R. & Desai, P., 1975. *Thermal expansion Metallic Elements and*
318   *Alloys-THERMOPHYSICAL PROPERTIES OF MATTER. VOLUME 12.* New York: SPRINGER
319   SCIENCE+BUSINESS MEDIA, LLC.

320   Walter, J. et al., 2014. *Multi-wire interconnection of busbar-free solar cells.* s.l., s.n., p. 380–388.

321   Zarmai, M. T., Ekere, N., Oduoza, C. & H. Amalu, E., 2016. Optimization of thermo-mechanical
322   reliability of solder joints in crystalline silicon solar cell assembly. *Microelectronics Reliability,* p. 117–
323   125.

324   Zhong, W., QIN , F., AN, T. & WANG, T., 2010. *Mechanical Properties of Intermetallic Compounds in*
325   *Solder Joints.* s.l., s.n.

326